Water-based Solar Cells Over 10% Efficiency: Designing Soft Nanoparticles for Improved Processability

Alexandre Holmes, Hugo Laval, Michele Guizzardi, Valentina Maruzzo, Giulia Folpini, Nadia Barbero, Elise Deniau-Lejeune, M. Schmutz, Sylvie Blanc, Annamaria Petrozza, et al.

▶ **To cite this version:**

Alexandre Holmes, Hugo Laval, Michele Guizzardi, Valentina Maruzzo, Giulia Folpini, et al.. Water-based Solar Cells Over 10% Efficiency: Designing Soft Nanoparticles for Improved Processability. Energy & Environmental Science, 2024, 17, pp.1107-1116. 10.1039/d3ee03744d . hal-04346806

HAL Id: hal-04346806
https://univ-pau.hal.science/hal-04346806v1

Submitted on 15 Dec 2023

HAL is a multi-disciplinary open access archive for the deposit and dissemination of scientific research documents, whether they are published or not. The documents may come from teaching and research institutions in France or abroad, or from public or private research centers.

L'archive ouverte pluridisciplinaire **HAL**, est destinée au dépôt et à la diffusion de documents scientifiques de niveau recherche, publiés ou non, émanant des établissements d'enseignement et de recherche français ou étrangers, des laboratoires publics ou privés.

Check for updates

View Article Online
View Journal

Energy & Environmental Science

Accepted Manuscript

This article can be cited before page numbers have been issued, to do this please use: A. Holmes, H. Laval, M. Guizzardi, V. Maruzzo, G. Folpini, N. Barbero, E. Deniau, M. Schmutz, S. Blanc, A. Petrozza, G. M. Paternò, G. Wantz, S. Chambon, C. Lartigau-Dagron and A. Bousquet, *Energy Environ. Sci.*, 2024, DOI: 10.1039/D3EE03744D.

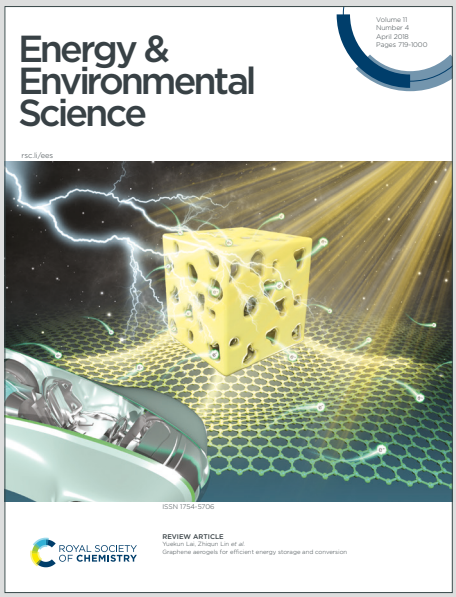

This is an Accepted Manuscript, which has been through the Royal Society of Chemistry peer review process and has been accepted for publication.

Accepted Manuscripts are published online shortly after acceptance, before technical editing, formatting and proof reading. Using this free service, authors can make their results available to the community, in citable form, before we publish the edited article. We will replace this Accepted Manuscript with the edited and formatted Advance Article as soon as it is available.

You can find more information about Accepted Manuscripts in the Information for Authors.

Please note that technical editing may introduce minor changes to the text and/or graphics, which may alter content. The journal's standard Terms & Conditions and the Ethical guidelines still apply. In no event shall the Royal Society of Chemistry be held responsible for any errors or omissions in this Accepted Manuscript or any consequences arising from the use of any information it contains.

ROYAL SOCIETY OF CHEMISTRY

rsc.li/ees

View Article Online
DOI: 10.1039/D3EE03744D

Published on 12 December 2023. Downloaded by CNRS - ICSN on 12/12/2023 8:52:16 PM.

Organic photovoltaics is a promising technology, giving access to lightweight, semitransparent and flexible devices with a low energy pay-back time. Recently, impressive improvements were achieved (up to 19% power conversion efficiencies – PCE – for a single-junction) thanks to the development of novel donor and acceptor semi-conducting materials for the active layer, which present complementary absorptions. These solar cells can be processed at a large-scale using printing and roll-to-roll industrial techniques. However, by considering environmental aspects, one limitation may come from the active layer deposition that uses organic (harmful) solvents. To address this issue, water-based inks can be prepared, in which the active materials are dispersed as nanoparticles. However, in order to form a homogeneous thin active layer film from nanoparticle assemblies, a thermal treatment is mandatory to ensure nanoparticle sintering. We show how the ink preparation technique is a key parameter to promote the formation of 'soft' nanoparticles (containing less crystallised materials) instead of 'hard' nanoparticles, allowing a sintering at an industrial compatible temperature (130°C instead of 200°C, respectively). Design of amorphous nanoparticles not only significantly reduced the processing temperatures, but also allowed to achieve high efficiencies for water-based solar cells up to 10% PCE.

Energy & Environmental Science Accepted Manuscript

View Article Online
DOI: 10.1039/D3EE03744D

Water-based Solar Cells Over 10% Efficiency: Designing Soft Nanoparticles for Improved Processability

Alexandre Holmes[1], Hugo Laval[2], Michele Guizzardi[3, 4], Valentina Maruzzo[1, 5], Giulia Folpini[3, 4], Nadia Barbero[5], Elise Deniau[1, 6], Marc Schmutz[7], Sylvie Blanc[1], Annamaria Petrozza[3, 4], Giuseppe Maria Paterno[3, 4], Guillaume Wantz[2], Sylvain Chambon[2]*, Christine Lartigau-Dagron[1]*, Antoine Bousquet[1]*

1. Université de Pau et Pays de l'Adour, E2S UPPA, CNRS, IPREM, Pau, France

2. Université de Bordeaux, CNRS, Bordeaux INP, IMS, UMR 5218, F-33400 Talence, France

3. Department of Physics, Politecnico di Milano, Milano 20133, Italy

4. Center for Nano Science and Technology@PoliMi, Istituto Italiano di Tecnologia, Milano 20134, Italy

5. University of Torino, Department of Chemistry, NIS Interdepartmental Centre and INSTM Reference Centre, Via Quarello 15a, 10135, Turin, Italy

6. Université du Mans, Institut des Molécules et Matériaux du Mans, UMR CNRS 6283, Le Mans, France

7. Université de Strasbourg, PLAMICS, CNRS, Institut Charles Sadron-UPR22, Strasbourg, France

Published on 12 December 2023. Downloaded by CNRS - ICSN on 12/12/2023 8:52:16 PM.

Energy & Environmental Science Accepted Manuscript

Abstract

Organic semiconductors are typically dissolved in organic solvents that are harmful to human health and the environment. To overcome this issue, these materials can be dispersed in water as nanoparticles to provide aqueous inks for more environmentally friendly solar cell manufacturing. Herein, we report the design of "soft" PTQ10:Y6 nanoparticles to decrease the annealing treatment (130°C/5 minutes) needed for processing the active layer and increase the conversion efficiency above 10%. Taking advantage of the nanoprecipitation mechanism, nanoparticles with intermixed donor/acceptor domains and a low degree of crystallinity were synthesized. Solar cells made with these nanoparticles were more efficient and needed less energy to be processed than those made from miniemulsion inks, in which Y6 crystallinity was more important. They even reached more than 90% of the performances of devices made from organic solvents, closing the gap with the classical toxic process.

View Article Online
DOI: 10.1039/D3EE03744D

Published on 12 December 2023. Downloaded by CNRS - ICSN on 12/12/2023 8:52:16 PM.

Energy & Environmental Science Accepted Manuscript

Introduction

Organic photovoltaics (OPV) has been a very promising candidate for energy generation in the last two decades, giving access to lightweight, semitransparent and flexible devices with a low energy pay-back time.[1–3] Finally, solar cell processing can be achieved at a large scale using printing and roll-to-roll techniques, making this technology compatible with industrial production.[4] The field has seen a renewed interest over the last 5 years due to impressive enhancements in power conversion efficiency and a stability expected to be over 15 years,[5] which can be attributed to the design of new acceptor materials (non-fullerene acceptors, NFA, improving absorption ranges) and nanomorphology control.[6–9] The current record of efficiency was set at 19.2% using a blend of donors mixed with a NFA.[10]

Active layer processing is usually achieved from an organic solution in which two materials (an electron donor and an electron acceptor material) are solubilized. However, most of the commonly used organic solvents in OPV are toxic, limiting processing at a large and industrial scale.[11] The use of more friendly solvents (such as tetrahydrofuran (THF) or *o*-xylene) slightly improved processing conditions, however they still present some toxicity toward both the environment and human health.[12,13] To solve this issue, a new branch of OPV focused on the generation of water-based inks to process the active layer,[14] in which donor and acceptor materials are dispersed as nanoparticles. Surfactants are introduced to provide stability to the nanoparticles which are highly hydrophobic and tend to aggregate. These stable dispersions can reach a solid content high enough (30-60 $mg.mL^{-1}$) for the processing of homogeneous active layers.[15] It is worth to mention that a few research teams have explored the use of media other than water, such as alcohols or acetonitrile.[16,17]

Two preparation techniques are mainly used to produce aqueous dispersions: miniemulsion and nanoprecipitation. There are fundamental differences between the mechanisms of each technique, influencing nanoparticle formation. In the case of the miniemulsion, the sonication of two immiscible phases first generates nanodroplets of active material solutions in a continuous water phase, followed by solvent evaporation to aggregate the active materials into nanoparticles. A surfactant is mandatory to produce stable nanodroplets. A wide range of organic solvents can be used, allowing the solubility of all kinds of conjugated materials and at a high concentration. The nanoparticle formation mechanism occurs on a relatively long timescale (few minutes/hours, **Figure 1**), providing enough time for the donor/acceptor/solvent to reach thermodynamic equilibrium. Therefore, a core-shell morphology has mostly been reported in the literature.[18] Although miniemulsion was largely represented in the literature (more than 80% of dispersion-based solar cells reported), efficiencies remained quite low (below 5%),[19,20] attributed to the unfavorable core-shell morphology. However, through careful selection of the donor:acceptor couple[21] or the surfactant molecule,[22] the core-shell

View Article Online
DOI: 10.1039/D3EE03744D

morphology can be prevented. For instance, Laval *et al.* recently reported a record efficiency of 9.98% for miniemulsion-based solar cells using PTQ10:Y6 NPs stabilized by SDS, with an optimized donor:acceptor morphology due to close interfacial energies.[23] A high annealing temperature of 200°C was, however, required to achieve homogeneous film formation and optimum performance. Such a high thermal treatment can be detrimental for large-scale production, both for energy consumption and viability of flexible substrates used in roll-to-roll industrial manufacturing.[24]

In the case of the nanoprecipitation methodology, the use of two miscible phases leads to rapid nanoparticle formation upon mixing. Its mechanism can be decomposed in two steps (nucleation and growth of the nuclei), which occur on a very short timescale of a few microseconds, leaving a short time for the active material to organize (**Figure 1**).[25] Even though the mechanism is fast, interactions of material/medium interfacial energies influence the main nanoparticle morphology. As a consequence, two morphologies have been reported, intermixed[26] and Janus.[15] Only a few examples of solar cells can be found in the literature, with extremely promising results attributed to a better nanoparticle morphology closer to a bulk heterojunction.[27] A record efficiency of up to 11% was achieved by Xie *et al.* using PM6:BTP-eC9 nanoparticles with the addition of 1,8-di-iodooctane (9% without) and a nonionic surfactant (pluronic F127).[28] Nevertheless, the design of additive-free water-based solar cells could help to avoid any risk to the environment or device stability.[29]

In this work, we designed 'soft' PTQ10:Y6 nanoparticles (s-NPs) by nanoprecipitation, in the sense that they showed a lower crystallinity than their counterparts synthesized by miniemulsion. Cryo-TEM, spectroscopy and calorimetry were used to prove the difference in Y6 crystallinity. Efficient exciton dissociation and long-lived charges in the microsecond time-regime were already observed in the dispersed state by transient absorption spectroscopy, revealing an optimized donor/acceptor morphology. Upon integration in devices, record efficiencies up to 10.14% were achieved for s-NPs with an optimal thermal annealing of 130°C. In comparison, a processing temperature of 200°C was needed for 'hard' nanoparticles (h-NPs, made *via* miniemulsion) and resulted in lower efficiencies (7.71%). We evidenced by atomic force microscopy how the melting/sintering of the nanoparticles influenced the final efficiencies. In optimized annealing conditions, higher performances for s-NPs were attributed to more suitable material distribution. As a promising competitive technology, these water-based devices achieved more than 90% of the performance of organic solvent reference devices (10.8%).

Published on 12 December 2023. Downloaded by CNRS - ICSN on 12/12/2023 8:52:16 PM.

Energy & Environmental Science Accepted Manuscript

View Article Online
DOI: 10.1039/D3EE03744D

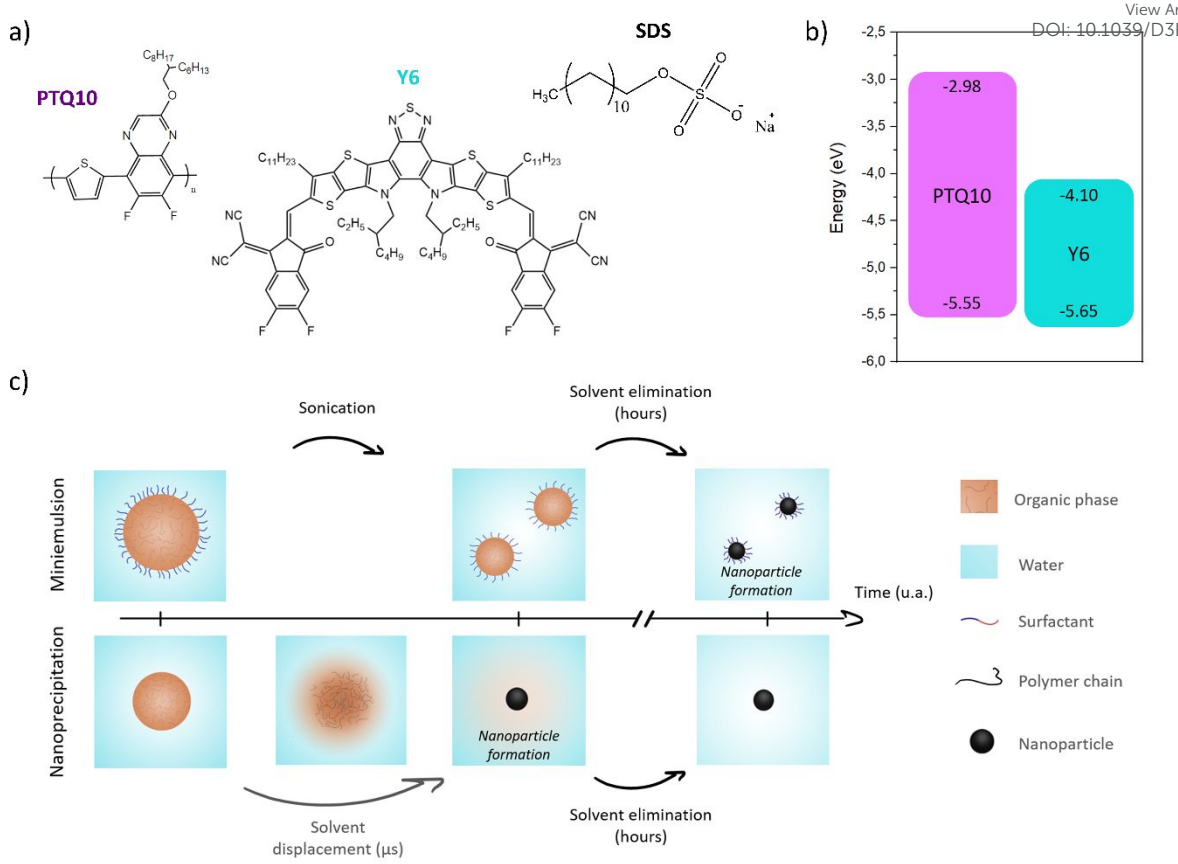

Figure 1. *(a) Chemical structure of active materials PTQ10 and Y6 and surfactant molecule (SDS). (b) Energetic levels of PTQ10 and Y6 materials. (c) Representative time scale of nanoparticle formation, depending on the preparation technique: hours for miniemulsion and less than seconds for nanoprecipitation. Modified with permission from [14]. Copyright 2021 American Chemical Society.*

Results and Discussion

Dispersed PTQ10:Y6 nanoparticles

Nanoparticles comprising the donor material PTQ10 (110 kg.mol^{-1}) and the acceptor Y6 were prepared using the nanoprecipitation technique in the presence of sodium dodecyl sulfate (SDS) as a surfactant. A 1:1.2 (mass ratio) of PTQ10:Y6 was first solubilized in THF and then added to the aqueous phase under vigorous stirring. For extensive comparison, PTQ10:Y6 nanoparticles were also prepared by miniemulsion with SDS as a surfactant, and the entire procedure is described in the supporting information. Both resulting dispersions showed an average particle size of 90 nm with high stability (Figure S1).

The UV–visible absorption spectrum of PTQ10:Y6 NPs prepared by nanoprecipitation showed the main features of PTQ10 with absorption maxima at 555 and 600 nm and of Y6 at 740 and 810 nm (**Figure 2**a). When prepared with the miniemulsion technique, a redshift of Y6 bands was observed (745 and

Published on 12 December 2023. Downloaded by CNRS - ICSN on 12/12/2023 8:52:16 PM.

Energy & Environmental Science Accepted Manuscript

View Article Online
DOI: 10.1039/D3EE03744D

822 nm) (**Figure 2**a) and could be attributed to larger and more crystalline domains.[30,31] As spectra were normalised at 815 nm on one absorption band of Y6, PTQ10 absorption is apparently higher in the 500-600 nm region in the case of miniemulsion. Indeed, as shown in Figure S2 (supplementary note 1), absorption behaviour of Y6 may be affected by the aggregation inside the nanoparticle.

Various morphologies, such as core-shell or Janus, have previously been obtained for nanoparticles formed by binary blended homopolymers from nanoprecipitation.[15,32,33] The resulting morphology was then predicted using dissipative particle and molecular dynamics simulations based on the surface tension between the materials, as well as between the materials and the surrounding liquid.[34,35] Materials showing similar interactions with the medium are expected to result in Janus nanoparticles, while a core-shell morphology would be promoted if one material showed a higher affinity with the medium than the other.

PTQ10 and Y6 surface energies, contact angles with the dispersive medium (water/THF/SDS) and calculated interfacial interactions can be found in the supplementary information (Table S1). According to the very close resulting interfacial interaction ratios, $\gamma_{PTQ10/dis}/\gamma_{PTQ10:Y6}$ = 2.7 and $\gamma_{Y6/dis}/\gamma_{PTQ10:Y6}$ = 3.3, a Janus morphology is expected for composite nanoparticles. Upon characterization by cryo-TEM, the exact morphology could not be identified (**Figure 2**b, Figure S3). The reason could be either a lack of contrast in Cryo-TEM images (electronic density of PTQ10 and Y6 being too close) or that the materials were homogeneously distributed due to their very close surface energies and interfacial interactions, $\gamma_{PTQ10:Y6}$ = 2.05 mN/m (refer to SI). As a result, a morphology close to intermixed could also be expected. However, one can very clearly observe the absence of any crystalline features in the cryo-TEM images of the nanoparticles made by nanoprecipitation.

Published on 12 December 2023. Downloaded by CNRS - ICSN on 12/12/2023 8:52:16 PM.

Energy & Environmental Science Accepted Manuscript

View Article Online
DOI: 10.1039/D3EE03744D

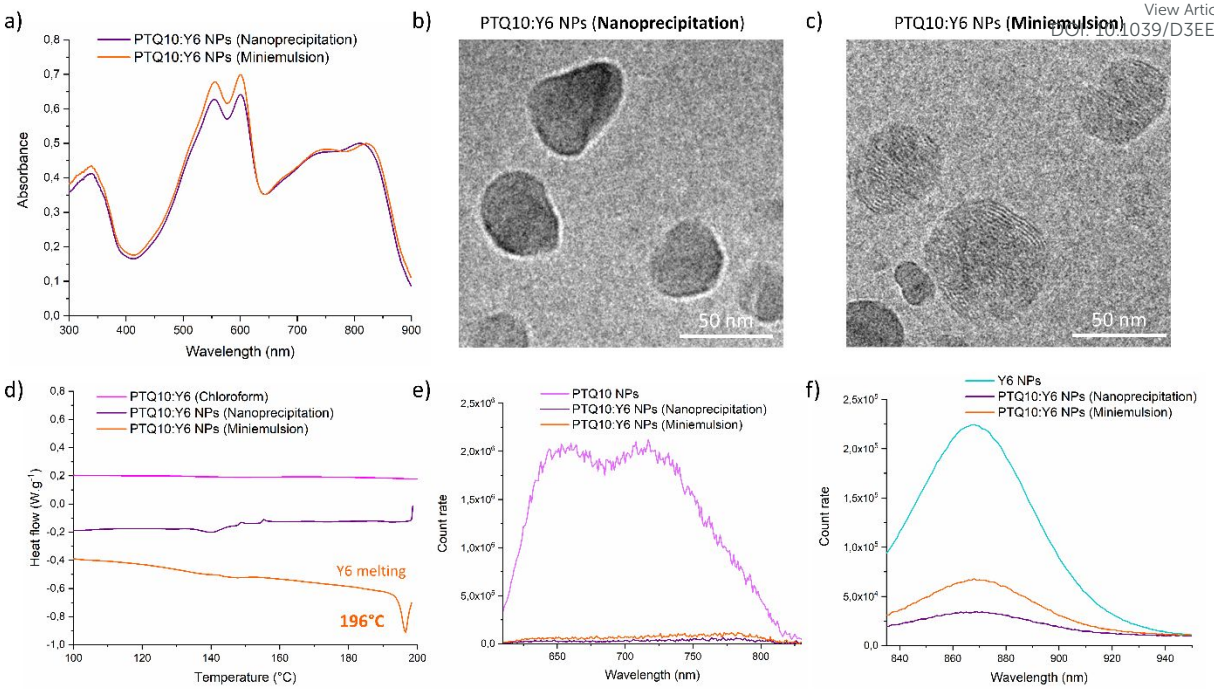

Figure 2. *(a) UV–visible absorption spectra of composite PTQ10:Y6 NPs prepared by nanoprecipitation and miniemulsion (stabilized by SDS) dispersed in water. Absorption profiles normalized on Y6 at 815 nm. Bright-field cryo-TEM images of (b) PTQ10:Y6 NPs prepared via nanoprecipitation and (c) PTQ10:Y6 NPs via miniemulsion. (d) Heating thermograms of the PTQ10:Y6 blend cast from chloroform and PTQ10:Y6 NPs, prepared either by nanoprecipitation or miniemulsion. All DSC experiments were performed under nitrogen at 20°C/min. Fluorescence emission spectra of (e) PTQ10 and PTQ10:Y6 NPs (excitation at 560 nm) and (f) Y6 and PTQ10:Y6 NPs (excitation at 812 nm) prepared by nanoprecipitation and miniemulsion.*

In the case of the dispersions made by miniemulsion, cryo-TEM images revealed highly crystalline nanoparticles (**Figure 2**c, Figure S3) with a lamellar spacing of 2.3 nm corresponding to Y6 crystals (Figure S4).[36] Even though no electronic contrast between the donor and acceptor was observed, crystalline features appeared all over the nanoparticle, suggesting a homogeneous repartition of Y6 nanodomains.

The degree of crystallinity in both dispersions was investigated by differential scanning calorimetry (DSC). For the raw materials, PTQ10 presented featureless thermograms in both heating and cooling ramps,[37] and pristine Y6 showed a melting peak at approximately 192°C upon heating (Figure S5) and a broad crystallization peak upon cooling at approximately 183°C (Figure S5). In comparison to pristine materials, thermograms of blends are dependent on the miscibility between both materials, in which high miscibility would result in decreased and/or shifted phase transitions.[38,39] For a PTQ10:Y6 blend (ratio 1:1.2) cast from chloroform, almost featureless thermograms are obtained (**Figure 2**d and Figure S6). The absence of Y6 melting upon heating and crystallization upon cooling ramps is attributed to a high intermixing of both materials, PTQ10 chains hindering Y6 ordering. PTQ10:Y6 nanoparticles prepared by nanoprecipitation presented an almost featureless thermogram (**Figure 2**d and Figure S6),

Published on 12 December 2023. Downloaded by CNRS - ICSN on 12/12/2023 8:52:16 PM.

Energy & Environmental Science Accepted Manuscript

View Article Online
DOI: 10.1039/D3EE03744D

extremely close to that of PTQ10:Y6 cast from chloroform. In contrast, in the case of miniemulsion-based dispersions, Y6 melting and crystallization features can be clearly identified, very similar to pristine Y6.

Cryo-TEM images, UV–visible absorption and DSC thermograms all show an increase in donor/acceptor intermixing and a decrease in Y6 crystallization when nanoprecipitation is used to produce nanoparticles in comparison to miniemulsion. As mentioned in the introduction, this behavior is linked with the time allowed for nanoparticle formation in the respective mechanism. Dispersions achieved from the miniemulsion needed high temperatures (196°C) to efficiently melt the Y6 crystalline domains distributed in the NPs. Therefore, they will be called 'hard' nanoparticles (h-NPs) in the rest of the manuscript. In contrast, the dispersion prepared by nanoprecipitation did not show any crystalline features and will be called 'soft' nanoparticles (s-NPs).

Photoluminescence experiments performed on both systems (hard and soft nanoparticles) showed a high quenching of PTQ10 fluorescence upon addition of Y6 in the nanoparticles, above 90% (**Figure 2**eA slightly higher quenching was measured for PTQ10:Y6 s-NPs (> 96%). No difference was observed for surfactant-free and SDS-stabilized dispersions (Figure S7), indicating that the presence of SDS did not impact the material distribution. When exciting the Y6 material (at 812 nm), its fluorescence was also quenched upon addition of PTQ10 (**Figure 2**f) in composite PTQ10:Y6 nanoparticles in comparison to the fluorescence of pristine Y6 nanoparticles. However, while dispersions prepared by nanoprecipitation presented a quenching of Y6 fluorescence over 82%, those prepared by miniemulsion showed only a quenching of approximately 67%. The lower charge transfer observed for PTQ10:Y6 h-NPs is also in agreement with a less intimate blend of donor and acceptor.

Since s-NPs presented an optimized morphology for charge generation, transient absorption spectroscopy (TAS) was performed to deeply understand their photophysics (Supplementary note).

The spectral evolution at several delay times of PTQ10 pristine s-NPs can be found in **Figure 3a**. By pumping at 550 nm, two photobleaching (PB) signals at 560 nm and 605 nm were identified, as well as a broad excited state absorption (ESA) band that extends from 620 nm to the low-energy end of our probed spectral window (540 – 950 nm). By exciting Y6 s-NPs at 800 nm, two PB broad bands centered at 670 nm and 850 nm (**Figure 3b**) were observed, and an extended ESA from 920 nm was observed.

Analyzing the PTQ10:Y6 s-NPs, the PB feature of the pristine PTQ10 s-NPs was still evidenced when pumping at 550 nm (**Figure 3c**), together with a positive signal at approximately 850 nm attributed to the bleaching of the Y6 material. In addition, an initial faster decay of the two PBs at 560 nm and 605 nm was observed. **Figure 3d** plots the decay dynamics at 605 nm for PTQ10 and PTQ10:Y6 s-NPs. A faster initial decay in the subpicosecond time regime was observed for the PTQ10:Y6 s-NPs, followed

Published on 12 December 2023. Downloaded by CNRS - ICSN on 12/12/2023 8:52:16 PM.

Energy & Environmental Science Accepted Manuscript

View Article Online
DOI: 10.1039/D3EE03744D

by a slower decay over the nanosecond time regime. The first fast component (fitting of decay dynamics can be found in Figure S8) can be attributed to an electron transfer from the donor to the acceptor, occurring before the picosecond, attested with a slow build-up of the signal at 850 nm (Figure S9). This transfer led to a long-lived charge separation that explains the second slower decay. Furthermore, by exciting in resonance with Y6 at 800 nm (**Figure 3e**), PB at 560 nm and 605 nm was still present even if the PTQ10 component was not excited. Such behavior can be related to ultrafast hole injection from Y6 to PTQ10, as sketched in **Figure 3g**. **Figure 3f** highlights the recombination dynamics at 605 nm of pristine Y6 NPs and PTQ10:Y6 NPs excited at 800 nm. In this case, a change in the dynamics at an early time delay can be observed due to ultrafast hole injection and an overall long-lived charge separation (> 1 ns), owing to charge separation that represented an additional bleaching mechanism of the ground state component. To resolve the dynamics of the charge-separated species, TAS on the ns-µs time scale was also performed by using a picosecond laser (Figure S10). Here, charges appeared to stay separated until the microsecond time regime. Specifically, in PTQ10:Y6 NPs, a third long-lived component (tau_3 = 0.6 µs, Figure S11b, c) can be observed, while a bi-exponential decay lasting approximately 100 ns was found in pristine NPs (Figure S11a). Both fitting and fitting results can be found in the supplementary information.

Published on 12 December 2023. Downloaded by CNRS - ICSN on 12/12/2023 8:52:16 PM.

Energy & Environmental Science Accepted Manuscript

View Article Online
DOI: 10.1039/D3EE03744D

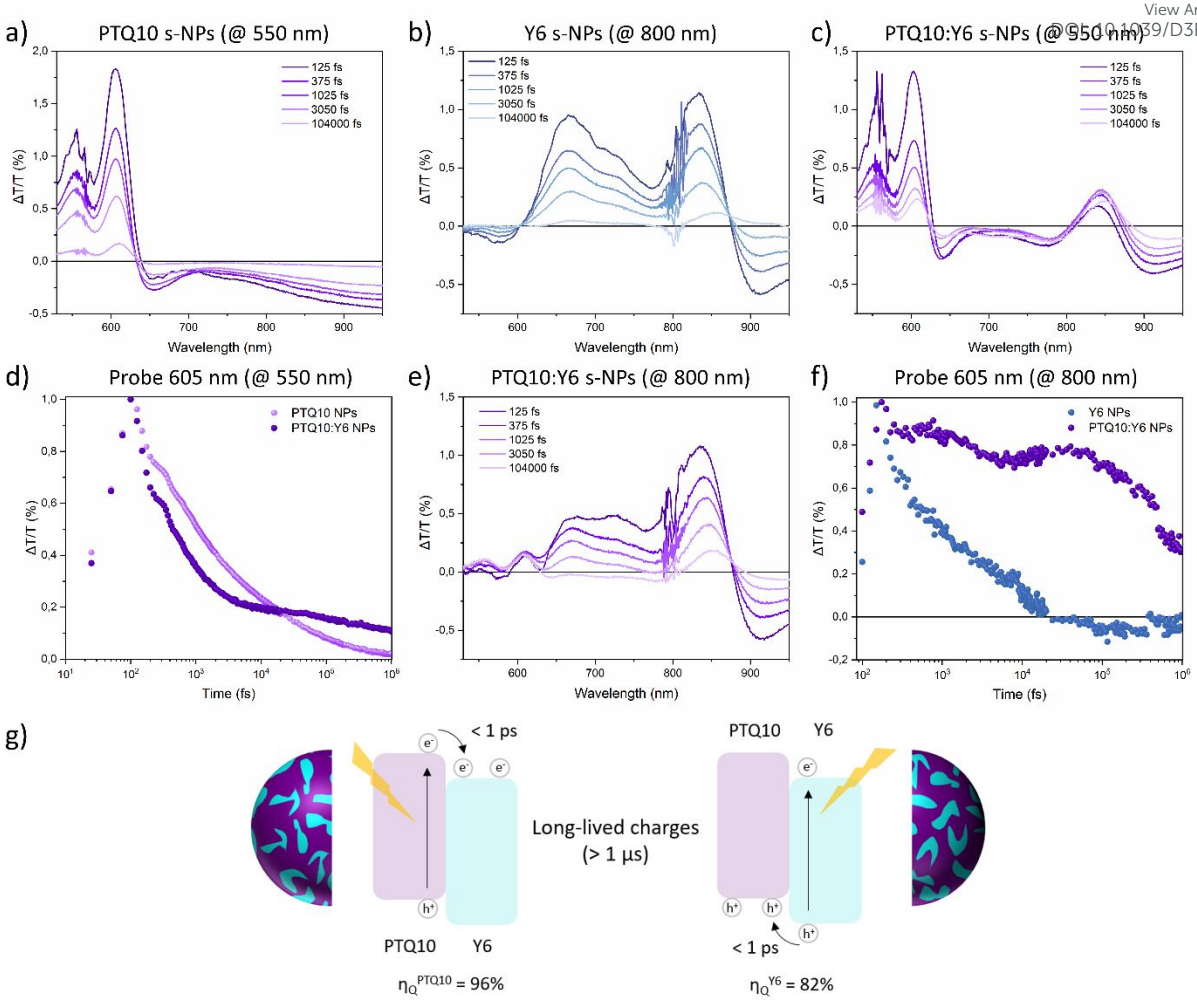

Figure 3. *Transient absorption spectra of pristine (a) PTQ10 nanoparticles (pumped at 550 nm), (b) Y6 nanoparticles (pumped at 800 nm) and (c) composite PTQ10:Y6 nanoparticles (pumped at 550 nm) at different time delays. (d) Comparison of transient absorption decay dynamics for PTQ10 and PTQ10:Y6 nanoparticles pumped at 550 nm and probed at 605 nm. (e) Transient absorption spectra of composite PTQ10:Y6 nanoparticles (pumped at 800 nm) at different time delays. (f) Comparison of transient absorption decay dynamics for Y6 and PTQ10:Y6 nanoparticles pumped at 800 nm and probed at 605 nm. (g) Scheme of charge generation inside PTQ10:Y6 nanoparticles for both materials. η_Q corresponds to the percentage of dissociated excitons in accordance with previous photoluminescence results for pristine materials.*

Thanks to an optimized morphology, PTQ10:Y6 nanoparticles prepared by nanoprecipitation promoted ultrafast dissociation in both PTQ10 and Y6 domains (**Figure 3g**), with higher charge transfer efficiency than those prepared by miniemulsion (η_Q, calculated from PL experiments, see detail of calculation in supplementary information). Furthermore, the formation of long-lived charges over the microsecond time-regime attested that the internal nanoparticle morphology was optimized toward charge separation and reduced recombination, already at the dispersed state. Such promising features are extremely valuable for photovoltaics and could also find applications in catalysis[36,40] or biomedical fields.[41,42]

Published on 12 December 2023. Downloaded by CNRS - ICSN on 12/12/2023 8:52:16 PM.

Energy & Environmental Science Accepted Manuscript

View Article Online
DOI: 10.1039/D3EE03744D

Published on 12 December 2023. Downloaded by CNRS - ICSN on 12/12/2023 8:52:16 PM.

Energy & Environmental Science Accepted Manuscript

Water-based organic solar cells

Prior to integration in devices, dispersions were submitted to filtration/centrifugation cycles to remove excess surfactant and increase the active material concentration. A final solid content of 60 mg.mL^{-1} was achieved without aggregation. Quantification of residual surfactant was performed by thermogravimetric analysis (Figure S12). After 5 centrifugation steps, a final residual content of SDS of approximately 11% was calculated from the mass loss measured at 220°C. This quantity was the minimum amount required to maintain colloidal stability since an additional centrifugation step led to destabilization and aggregation.

Organic solar cells were prepared from aqueous inks using an inverted architecture (glass/ITO/ZnO/PTQ10:Y6/MoO_3/Ag), and the full procedure can be found in the supplementary information. After deposition of the ZnO layer on Glass/ITO substrates, the latter were treated with UV-O_3 for 20 minutes to increase the wettability of the ZnO layer upon deposition and ensure good film formation for the active layer processed from dispersions. Deposition of the PTQ10:Y6 aqueous ink was achieved through a one-step spin-coating process. Thermal treatment was first optimized with different annealing temperatures for 2 minutes, and the evolution of the overall PV parameters is reported in **Table 1** and Figure S13. At an initial annealing temperature of 100°C, a PCE of 6.4% was achieved, but an optimum thermal treatment of 130°C resulted in efficiencies raising up to 7.9%, mainly explained by an increased J_{SC}. Higher annealing temperatures resulted in a decrease in the photovoltaics parameters, affecting J_{SC} and FF mainly, reaching a plateau in efficiency of approximately 5.5%.

***Table 1**. Evolution of photovoltaic parameters of PTQ10:Y6 s-NP devices prepared by nanoprecipitation for different annealing temperatures. Annealing was performed for 2 minutes under a nitrogen atmosphere prior to electrode deposition. Active layer thickness of 180 nm. Average values and standard deviations calculated from at least 6 devices*

Solvent	Annealing Temperature (°C)	Jsc (mA.cm^{-2})	Voc (mV)	FF (%)	PCE[a]
Water (SDS)	100	17.8 ± 1.6	719 ± 1	50 ± 1	6.41% (7.17%)
	130	**19.1 ± 1.0**	**732 ± 9**	**51 ± 2**	**7.16% (7.87%)**
	150	17.1 ± 1.0	732 ± 9	45 ± 1	5.64% (6.36%)
	170	16.4 ± 1.0	722 ± 14	47 ± 1	5.54% (6.09%)
	200	17.2 ± 0.0	718 ± 13	44 ± 1	5.40% (5.72%)

[a] The best device performance is shown in brackets

Optimization of the active layer thickness from 180 to 140 nm and annealing time from 2 to 5 minutes resulted in improved J_{SC} (up to 21 mA.cm^{-2}) and efficiencies up to 8.6% (Table S2, Table S3). However,

View Article Online
DOI: 10.1039/D3EE03744D

the devices still suffered from low FF parameters (54%). As the FF is driven by the competition between charge recombination and extraction from the active layer to the corresponding charge transporting layer/electrode, the film morphology/homogeneity strongly affects this parameter.[43] After preparation through centrifugal dialysis, dispersions were filtered to avoid the presence of large objects and were stored before use. No aggregation was observed from DLS experiments and UV–visible spectra (Figure S14), with dispersions stable for more than several weeks. However, the formation of few aggregates, below the limit of detection, may affect film formation and photovoltaic performance. Destouesse *et al.* highlighted that the presence of defects and pinholes in the active layer film can lead to a strong decrease in photovoltaic performance.[44] Additionally, commercial colloidal dispersions such as PEDOT-PSS require filtration prior to use to prevent poor film formation due to the presence of a few large aggregates.

To properly understand the importance of the delay between filtration and deposition, solar cells were processed a few minutes, 1 day and 1 week after filtration on a 0.45 µm cellulose filter. As shown in **Figure 4a, b**, the overall film homogeneity was strongly improved when the deposition occurred a few minutes after filtration. On the other hand, when the delay between filtration and deposition increased to 1 day or 1 week, the number of defects and aggregates consequently increased. Even at the microscale, the presence of a few aggregates resulted in films with numerous defects.

An impressive improvement in all the parameters was achieved for the dispersion filtered only a few minutes prior to deposition (**Figure 4c** and Table S4), with efficiencies up to 10.14%, a high J_{SC} of 22.51 mA.cm^{-2}, a V_{OC} of 757 mV and an FF of 60%. Upon decreasing the time delay between filtration and deposition, the FF followed successive improvements from 51% to 54% and finally 59% (**Figure 4c**). Not only the FF but also both J_{SC} and V_{OC} showed an improvement for the dispersion processed immediately after filtration, thanks to an optimized film morphology. To the best of our knowledge, such performances are a record for water-based devices without any additive.

Published on 12 December 2023. Downloaded by CNRS - ICSN on 12/12/2023 8:52:16 PM.

Energy & Environmental Science Accepted Manuscript

View Article Online
DOI: 10.1039/D3EE03744D

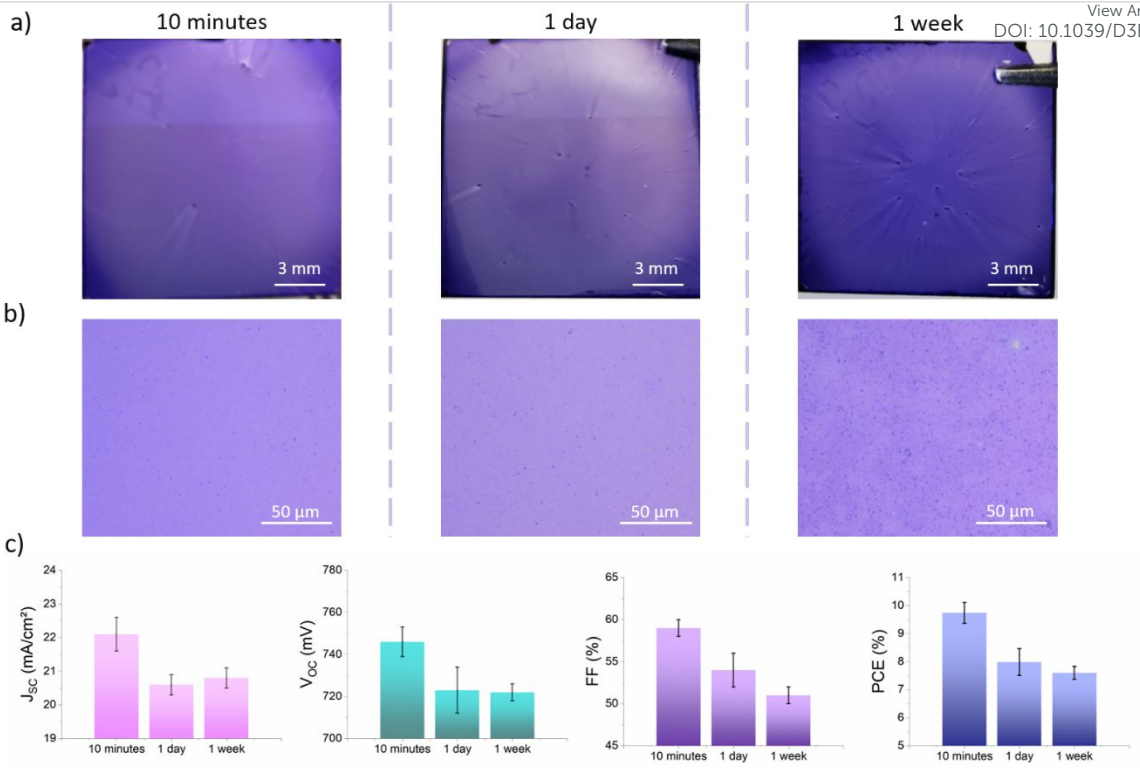

Figure 4. *(a) Photographs and (b) optical microscopy images of PTQ10:Y6 NP films from nanoprecipitation showing the evolution of film homogeneity upon time processing for 10 minutes, 1 day or 1 week after filtration on a 0.45 µm cellulose filter. (c) Evolution of photovoltaic parameters (short-circuit current density J_{SC}, open-circuit voltage V_{OC}, fill factor FF and power conversion efficiency PCE) with filtration time prior to deposition. Average on at least 6 devices.*

When integrating PTQ10:Y6 h-NPs (made *via* miniemulsion) into devices, a maximum efficiency of 7.71% was achieved **(Table 2**), with an optimized annealing temperature of 200°C and filtration prior to processing (Table S5). In comparison to the Laval *et al.* study, lower performances were achieved, mainly due to lower J_{SC} and FF. This difference can be explained by the change in PTQ10 molar mass (60 kg.mol^{-1} in Laval *et al.*[23], versus 110 kg.mol^{-1} herein), resulting in lower intermolecular diffusion of Y6 in PTQ10 domains. Nevertheless, the same thermal treatment (200°C) was required to achieve the highest performances.

Table 2. Photovoltaic parameters of PTQ10:Y6 devices processed from aqueous dispersions and chloroform. Thermal treatments were optimized for each condition under a nitrogen atmosphere prior to electrode deposition. All active layers are 140 nm thick. Average values and standard deviations calculated from at least 6 devices. 's-NPs' and 'h-NPs' stand for nanoprecipitation- and miniemulsion-based dispersions, respectively.

Published on 12 December 2023. Downloaded by CNRS - ICSN on 12/12/2023 8:52:16 PM.

Energy & Environmental Science Accepted Manuscript

View Article Online
DOI: 10.1039/D3EE03744D

Solvent	Dispersion	Annealing (°C)	Jsc (mA.cm^{-2})	Voc (mV)	FF (%)	PCE[a]
Water (SDS)	**s-NPs**	**130°C**	**22.1 ± 0.5**	**746 ± 7**	**59 ± 1**	**9.74% (10.14%)**
	h-NPs	200°C	18.0 ± 0.2	695 ± 5	59 ± 2	7.32% (7.71%)
Chloroform	-	100°C	24.7 ± 0.5	768 ± 21	57 ± 3	10.79% (11.61%)

[a] The best device performance is shown in brackets

Regardless of the device efficiency, a strong difference in the thermal treatment required to reach the highest performance can be noted. A closer look at the active layer nanomorphology evolution upon annealing revealed the strength of s-NPs. Atomic force microscopy (AFM) (**Figure 5**, Figure S15) showed that even without annealing, s-NPs were already slightly sintered but still presented a discrete nanoparticle shape and grain boundaries, which can limit charge transport.[45] Annealing at 100°C helped to improve nanoparticle interconnection, but an optimum morphology was achieved at 130°C, with lower roughness (r_Q) and complete loss of nanoparticle shape. A further increase in the annealing temperature increased the material segregation, resulting in larger domains and affecting the J_{SC} and FF parameters. The unoptimized morphology could be attested by the appearance of heterogeneities at the macroscale (Figure S16) and a slight redshift observed for the Y6 absorption peak, from 825 to 835 nm (Figure S17).

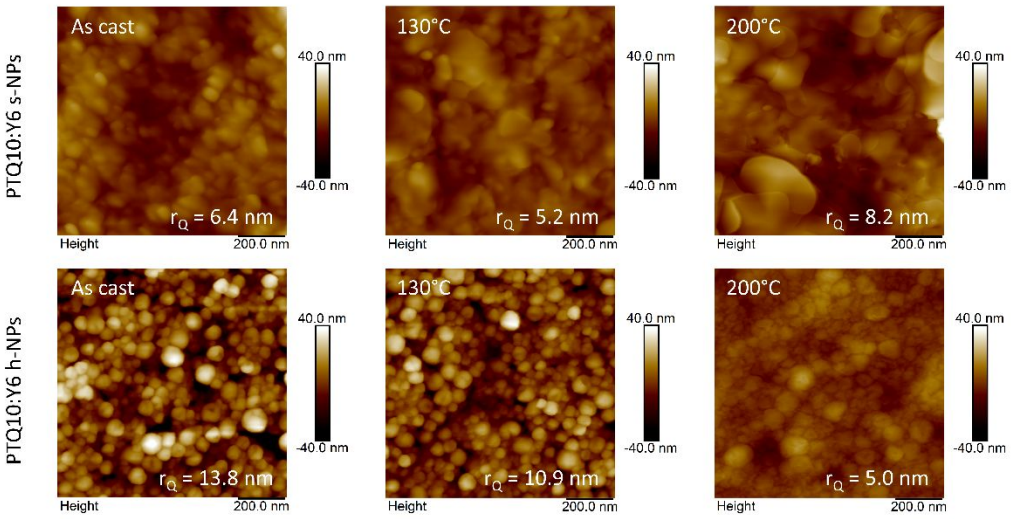

***Figure 5**. AFM height images of PTQ10:Y6 NP-based active layers at different annealing temperatures, prepared either by nanoprecipitation (s-NPs) or miniemulsion (h-NPs). The film roughness r_Q is presented at the bottom of each image.*

Published on 12 December 2023. Downloaded by CNRS - ICSN on 12/12/2023 8:52:16 PM.

Energy & Environmental Science Accepted Manuscript

View Article Online
DOI: 10.1039/D3EE03744D

In contrast, PTQ10:Y6 h-NPs showed very well-defined nanoparticle shapes on the as-cast films (**Figure 5**, Figure S18). When using an annealing temperature of 130°C, almost no evolution of the film morphology was identified, with nanoparticles showing no interparticle connections and a higher film roughness. The sintering of h-NPs was only achieved after annealing at 200°C, reducing the roughness of the active layer.

Correlating the nanoparticle features highlighted in the dispersed state and their behavior once processed as an active layer, there is a direct relationship between the crystallinity and the annealing temperature required to achieve the formation of a homogeneous film. The presence of highly crystalline Y6 domains within PTQ10:Y6 h-NPs made their sintering difficult to achieve, and Y6 crystallites acted as a shield protecting nanoparticle integrity (melting temperature approximately 196°C). The necessity to use an annealing temperature of 200°C might result in enhanced material segregation, leading to lower J_{SC} and V_{OC} values. In contrast, nanoparticles with low crystallinity Y6 enabled the use of a lower annealing temperature that led to more efficient devices presenting an optimized donor/acceptor morphology, attributed to a higher J_{SC}.[46,47]

Devices prepared from s-NPs were finally compared to reference devices cast from chloroform. The performances were quite close, with average PCEs of 9.74% and 10.79%, respectively (**Table 2**, **Figure 6a**). The slightly lower V_{OC} values could be explained by the formation of a less homogeneous film, presenting a few defects, in comparison to the highly homogeneous layers cast from chloroform. Both presented maximum FF around 60%, a lower value than what can be found in the literature.[48] This discrepancy can be attributed to unoptimized ZnO layer and/or architecture. However, water-based devices achieved FF at least as high as those fabricated from chloroform, indicating therefore similar charge transport properties in both kinds of active layers.

To investigate the difference in J_{SC}, external quantum efficiency (EQE) experiments were conducted on NP-based and chloroform-based devices (**Figure 6b**). The overall shapes of the EQE spectra for s-NPs and chloroform-cast devices were quite similar, with high contributions from PTQ10 and Y6 materials. In the case of devices processed from h-NPs, the EQE spectrum is coherent with lower performances, with an overall weaker photocurrent. For devices prepared by s-NPs or chloroform, while the PTQ10 contribution was identified as similar (up to 75%), the contribution from 600 to 1000 nm, attributed to Y6, was found to be slightly lower for water-based devices (64% *vs* 70%). The high contribution from PTQ10 shows that charges can be efficiently generated and extracted from the PTQ10 domains, consistent with the high PL quenching observed in the nanoparticle state. As we observed long-lived charges in the s-NPs, the lower contribution of Y6 was attributed to the presence of larger domains, increasing geminate recombination.

Published on 12 December 2023. Downloaded by CNRS - ICSN on 12/12/2023 8:52:16 PM.

Energy & Environmental Science Accepted Manuscript

View Article Online
DOI: 10.1039/D3EE03744D

Published on 12 December 2023. Downloaded by CNRS - ICSN on 12/12/2023 8:52:16 PM.

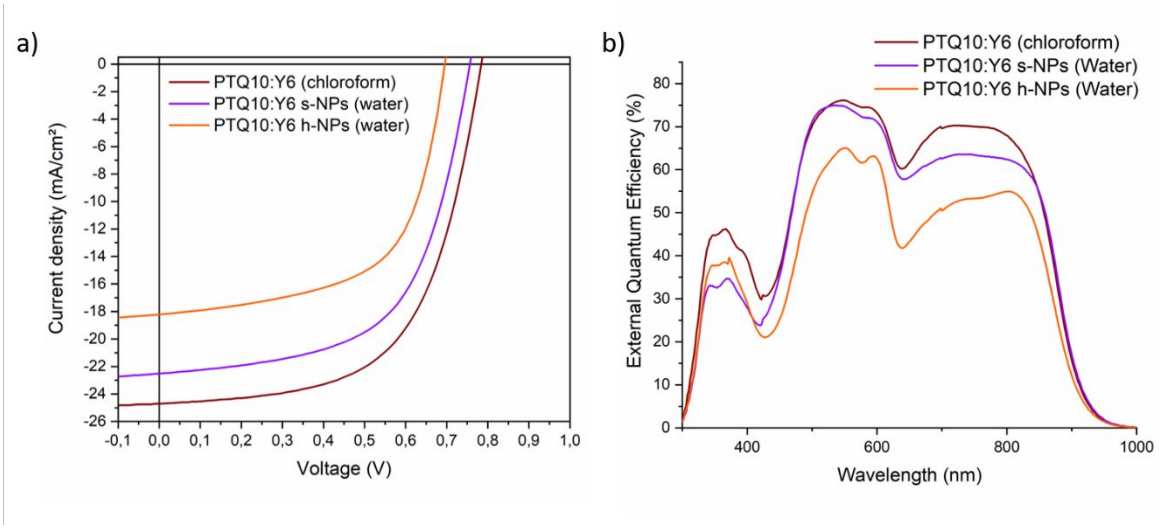

Figure 6. (a) J-V curves and (b) EQE spectra of PTQ10:Y6 devices prepared by chloroform or aqueous dispersions stabilized by SDS. All devices were prepared under optimized conditions.

Conclusion

PTQ10:Y6 nanoparticles stabilized by SDS were prepared using two different preparation techniques, miniemulsion and nanoprecipitation, with a focus on the latter. Relying on the formation mechanism of nanoparticles through nanoprecipitation, and especially the short time allowed for materials to self-organize, soft nanoparticles (s-NPs) were synthesized with a low crystallinity of Y6 material and a high degree of intermixing between both materials. Moreover, s-NPs displayed excellent photophysical properties with ultrafast charge generation (subpicosecond) and the formation of long-lived charges in the microsecond time-regime. Once integrated in devices, s-NPs showed the advantage of requiring a lower annealing temperature (130°C) while leading to higher performance (10.14%) than their h-NP counterparts prepared by miniemulsion (200°C, 7.71%). A direct link between the annealing temperature and crystalline behavior was established by the characterization of the initial aqueous dispersions and the AFM study of film morphology upon thermal treatment. In water-based inks, control of the crystalline behavior appears to be a critical factor to avoid high processing temperatures since nanoparticle sintering is mandatory to achieve high efficiencies. Reduction of crystallinity through selection of the preparation technique limiting crystallization or the use of amorphous materials are ways to explore.

The nanoprecipitation technique not only remains extremely simple for large-scale transfer with continuous flow production,[49] but the absence of additives and the use of lower temperatures are also attractive for industrial manufacturing and/or the use of flexible substrates. To conclude, green and

Energy & Environmental Science Accepted Manuscript

View Article Online
DOI: 10.1039/D3EE03744D

efficient water-based organic solar cells were prepared, with an average efficiency reaching more than 90% of the average performance from organic solvent references (10.8%).

Experimental section

Experimental details for nanoparticle preparation, characterization and introduction into organic solar cells are described in supplementary information.

Conflicts of interest

The authors declare no conflicts of interest.

Acknowledgements

The authors thanks ISIFoR through the NAJA-H2 and PyJAMA project and also the CNRS 80-PRIME 2023 program through ECOSOLORG for funding part of this research. The authors acknowledge the support provided by the ANR through the WATER-PV project N°ANR-20-CE05-0002. The authors also thank UNITA alliance and UPPA for the funding of V. M. and the Grant for Internationalization (GFI), Programmazione Triennale 21-23, "Green technologies: renewable energies and the green transition". G. F. and A. P. acknowledge the funding from the European Union's Horizon 2020 research and innovation program through the ERC project SOPHY under Grant Agreement No. 771528.

References

1 Y. Li, G. Xu, C. Cui and Y. Li, *Adv. Energy Mater.*, 2018, **8**, 1701791.

2 N. Espinosa, R. García-Valverde, A. Urbina and F. C. Krebs, *Sol. Energy Mater. Sol. Cells*, 2011, **95**, 1293–1302.

3 H. Yu, J. Wang, Q. Zhou, J. Qin, Y. Wang, X. Lu and P. Cheng, *Chem. Soc. Rev.*, 2023, **52**, 4132–4148.

4 S. Berny, N. Blouin, A. Distler, H.-J. Egelhaaf, M. Krompiec, A. Lohr, O. R. Lozman, G. E. Morse, L. Nanson, A. Pron, T. Sauermann, N. Seidler, S. Tierney, P. Tiwana, M. Wagner and H. Wilson, *Adv. Sci.*, 2016, **3**, 1500342.

5 X. Du, T. Heumueller, W. Gruber, A. Classen, T. Unruh, N. Li and C. J. Brabec, *Joule*, 2019, **3**, 215–226.

6 C. Yan, S. Barlow, Z. Wang, H. Yan, A. K.-Y. Jen, S. R. Marder and X. Zhan, *Nat. Rev. Mater.*, 2018, **3**, 18003.

7 X. Li, F. Pan, C. Sun, M. Zhang, Z. Wang, J. Du, J. Wang, M. Xiao, L. Xue, Z.-G. Zhang, C. Zhang, F. Liu and Y. Li, *Nat. Commun.*, 2019, **10**, 519.

Published on 12 December 2023. Downloaded by CNRS - ICSN on 12/12/2023 8:52:16 PM.

Energy & Environmental Science Accepted Manuscript

View Article Online
DOI: 10.1039/D3EE03744D

Published on 12 December 2023. Downloaded by CNRS - ICSN on 12/12/2023 8:52:16 PM.

8 Y. Lin, J. Wang, Z.-G. Zhang, H. Bai, Y. Li, D. Zhu and X. Zhan, *Adv. Mater.*, 2015, **27**, 1170–1174.

9 J. Wang, P. Xue, Y. Jiang, Y. Huo and X. Zhan, *Nat. Rev. Chem.*, 2022, **6**, 614–634.

10 L. Zhu, M. Zhang, J. Xu, C. Li, J. Yan, G. Zhou, W. Zhong, T. Hao, J. Song, X. Xue, Z. Zhou, R. Zeng, H. Zhu, C.-C. Chen, R. C. I. MacKenzie, Y. Zou, J. Nelson, Y. Zhang, Y. Sun and F. Liu, *Nat. Mater.*, 2022, **21**, 656–663.

11 X. Zhou, W. Belcher and P. Dastoor, *Polymers*, 2014, **6**, 2832–2844.

12 S. Lee, D. Jeong, C. Kim, C. Lee, H. Kang, H. Y. Woo and B. J. Kim, *ACS Nano*, 2020, **14**, 14493–14527.

13 Z. Ma, B. Zhao, Y. Gong, J. Deng and Z. Tan, *J. Mater. Chem. A*, 2019, **7**, 22826–22847.

14 A. Holmes, E. Deniau, C. Lartigau-Dagron, A. Bousquet, S. Chambon and N. P. Holmes, *ACS Nano*, 2021, **15**, 3927–3959.

15 A. Holmes, H. Laval, M. Schmutz, S. Blanc, J. Allouche, B. Watts, G. Wantz, N. P. Holmes, K. Hirakawa, E. Deniau, S. Chambon, C. Lartigau-Dagron and A. Bousquet, *Mater. Today Chem.*, 2022, **26**, 101229.

16 F. Manger, K. Fischer, P. Marlow, H. Röhm, C. Sprau and A. Colsmann, *Adv. Energy Mater.*, 2023, **13**, 2202820.

17 F. Manger, P. Marlow, F. Karen, M. Nöller, C. Sprau and A. Colsmann, *Adv. Funct. Mater.*, 2022, **32**, 2202566.

18 I. Persson, H. Laval, S. Chambon, G. Bonfante, K. Hirakawa, G. Wantz, B. Watts, M. A. Marcus, X. Xu, L. Ying, G. Lakhwani, M. R. Andersson, J. M. Cairney and N. P. Holmes, *Nanoscale*, 2023, **15**, 6126–6142.

19 S. Gärtner, M. Christmann, S. Sankaran, H. Röhm, E.-M. Prinz, F. Penth, A. Pütz, A. E. Türeli, B. Penth, B. Baumstümmler and A. Colsmann, *Adv. Mater.*, 2014, **26**, 6653–6657.

20 L. D'Olieslaeger, G. Pirotte, I. Cardinaletti, J. D'Haen, J. Manca, D. Vanderzande, W. Maes and A. Ethirajan, *Org. Electron.*, 2017, **42**, 42–46.

21 M. G. Barr, S. Chambon, A. Fahy, T. W. Jones, M. A. Marcus, A. L. D. Kilcoyne, P. C. Dastoor, M. J. Griffith and N. P. Holmes, *Mater. Chem. Front.*, 2021, **5**, 2218–2233.

22 R. Chowdhury, N. P. Holmes, N. Cooling, W. J. Belcher, P. C. Dastoor and X. Zhou, *ACS Omega*, 2022, **7**, 9212–9220.

23 H. Laval, A. Holmes, M. A. Marcus, B. Watts, G. Bonfante, M. Schmutz, E. Deniau, R. Szymanski, C. Lartigau-Dagron, X. Xu, J. M. Cairney, K. Hirakawa, F. Awai, T. Kubo, G. Wantz, A. Bousquet, N. P. Holmes and S. Chambon, *Adv. Energy Mater.*, 2023, 2300249.

24 I. McCulloch, M. Chabinyc, C. Brabec, C. B. Nielsen and S. E. Watkins, *Nat. Mater.*, 2023, DOI:10.1038/s41563-023-01579-0.

25 K. N. Schwarz, S. B. Farley, T. A. Smith and K. P. Ghiggino, *Nanoscale*, 2015, **7**, 19899–19904.

26 D. Darwis, N. Holmes, D. Elkington, A. L. David Kilcoyne, G. Bryant, X. Zhou, P. Dastoor and W. Belcher, *Sol. Energy Mater. Sol. Cells*, 2014, **121**, 99–107.

27 C. Xie, T. Heumüller, W. Gruber, X. Tang, A. Classen, I. Schuldes, M. Bidwell, A. Späth, R. H. Fink, T. Unruh, I. McCulloch, N. Li and C. J. Brabec, *Nat. Commun.*, 2018, **9**, 5335.

28 C. Xie, S. Liang, G. Zhang and S. Li, *Polymers*, 2022, **14**, 4229.

Energy & Environmental Science Accepted Manuscript

View Article Online
DOI: 10.1039/D3EE03744D

29 N. Y. Doumon, G. Wang, X. Qiu, A. J. Minnaard, R. C. Chiechi and L. J. A. Koster, *Sci Rep.*, 2019, **9**, 4350.

30 S. Dong, T. Jia, K. Zhang, J. Jing and F. Huang, *Joule*, 2020, **4**, 2004–2016.

31 J. Xue, H. B. Naveed, H. Zhao, B. Lin, Y. Wang, Q. Zhu, B. Wu, Z. Bi, X. Zhou, C. Zhao, K. Zhou and W. Ma, *J. Mater. Chem. A*, 2022, **10**, 13439–13447.

32 T. Higuchi, A. Tajima, H. Yabu and M. Shimomura, *Soft Matter*, 2008, **4**, 1302.

33 C. Sosa, R. Liu, C. Tang, F. Qu, S. Niu, M. Z. Bazant, R. K. Prud'homme and R. D. Priestley, *Macromolecules*, 2016, **49**, 3580–3585.

34 N. Li, A. Z. Panagiotopoulos and A. Nikoubashman, *Langmuir*, 2017, **33**, 6021–6028.

35 H. Guo, X. Qiu and J. Zhou, *The Journal of Chemical Physics*, 2013, **139**, 084907.

36 J. Kosco, S. Gonzalez-Carrero, C. T. Howells, T. Fei, Y. Dong, R. Sougrat, G. T. Harrison, Y. Firdaus, R. Sheelamanthula, B. Purushothaman, F. Moruzzi, W. Xu, L. Zhao, A. Basu, S. De Wolf, T. D. Anthopoulos, J. R. Durrant and I. McCulloch, *Nat. Energy*, 2022, **7**, 340–351.

37 T. Zhang, M. Moser, A. D. Scaccabarozzi, H. Bristow, P. Jacoutot, A. Wadsworth, T. D. Anthopoulos, I. McCulloch and N. Gasparini, *J. Phys. Mater.*, 2021, **4**, 045001.

38 D. Baran, R. S. Ashraf, D. A. Hanifi, M. Abdelsamie, N. Gasparini, J. A. Röhr, S. Holliday, A. Wadsworth, S. Lockett, M. Neophytou, C. J. M. Emmott, J. Nelson, C. J. Brabec, A. Amassian, A. Salleo, T. Kirchartz, J. R. Durrant and I. McCulloch, *Nat. Mater.*, 2017, **16**, 363–369.

39 C. Yang, S. Zhang, J. Ren, M. Gao, P. Bi, L. Ye and J. Hou, *Energy Environ. Sci.*, 2020, **13**, 2864–2869.

40 N. P. Holmes, S. Chambon, A. Holmes, X. Xu, K. Hirakawa, E. Deniau, C. Lartigau-Dagron and A. Bousquet, *Curr. Opin. Colloid Interface Sci.*, 2021, **56**, 101511.

41 T. C. De Souza-Guerreiro, G. Bondelli, I. Grobas, S. Donini, V. Sesti, C. Bertarelli, G. Lanzani, M. Asally and G. M. Paternò, *Adv. Science*, 2023, **10**, 2205007.

42 M. L. DiFrancesco, F. Lodola, E. Colombo, L. Maragliano, M. Bramini, G. M. Paternò, P. Baldelli, M. D. Serra, L. Lunelli, M. Marchioretto, G. Grasselli, S. Cimò, L. Colella, D. Fazzi, F. Ortica, V. Vurro, C. G. Eleftheriou, D. Shmal, J. F. Maya-Vetencourt, C. Bertarelli, G. Lanzani and F. Benfenati, *Nat. Nanotechnol.*, 2020, **15**, 296–306.

43 D. Bartesaghi, I. del C. Pérez, J. Kniepert, S. Roland, M. Turbiez, D. Neher and L. J. A. Koster, *Nat. Commun.*, 2015, **6**, 7083.

44 E. Destouesse, S. Chambon, S. Courtel, L. Hirsch and G. Wantz, *ACS Appl. Mater. Interfaces*, 2015, **7**, 24663–24669.

45 N. P. Holmes, M. Marks, P. Kumar, R. Kroon, M. G. Barr, N. Nicolaidis, K. Feron, A. Pivrikas, A. Fahy, A. D. de Z. Mendaza, A. L. D. Kilcoyne, C. Müller, X. Zhou, M. R. Andersson, P. C. Dastoor and W. J. Belcher, *Nano Energy*, 2016, **19**, 495–510.

46 F. Piersimoni, S. Chambon, K. Vandewal, R. Mens, T. Boonen, A. Gadisa, M. Izquierdo, S. Filippone, B. Ruttens, J. D'Haen, N. Martin, L. Lutsen, D. Vanderzande, P. Adriaensens and J. V. Manca, *J. Phys. Chem. C*, 2011, **115**, 10873–10880.

47 K. Vandewal, W. D. Oosterbaan, S. Bertho, V. Vrindts, A. Gadisa, L. Lutsen, D. Vanderzande and J. V. Manca, *Appl. Phys. Lett.*, 2009, **95**, 123303.

Published on 12 December 2023. Downloaded by CNRS - ICSN on 12/12/2023 8:52:16 PM.

Energy & Environmental Science Accepted Manuscript

View Article Online
DOI: 10.1039/D3EE03744D

48 B. Qiu, S. Chen, C. Sun, J. Yuan, X. Zhang, C. Zhu, S. Qin, L. Meng, Y. Zhang, C. Yang, Y. Zou and Y. Li, *Sol. RRL*, 2020, **4**, 1900540.

49 K. Fischer, P. Marlow, F. Manger, C. Sprau and A. Colsmann, *Adv. Mater. Technol.*, 2022, 2200297.

Published on 12 December 2023. Downloaded by CNRS - ICSN on 12/12/2023 8:52:16 PM.

Energy & Environmental Science Accepted Manuscript